Elucidation of the trigonelline degradation pathway reveals previously undescribed enzymes and metabolites

Nadia Perchat, Pierre-Loïc Saaidi, Ekaterina Darii, Christine Pellé, Jean-Louis Petit, Marielle Besnard-Gonnet, Véronique de Berardinis, Maeva Dupont, Alexandra Gimbernat, Marcel Salanoubat, et al.

Elucidation of the trigonelline degradation pathway reveals previously undescribed enzymes and metabolites

Nadia Perchat[a,1], Pierre-Loïc Saaidi[a,1], Ekaterina Darii[a], Christine Pellé[a], Jean-Louis Petit[a], Marielle Besnard-Gonnet[a], Véronique de Berardinis[a], Maeva Dupont[a], Alexandra Gimbernat[a], Marcel Salanoubat[a], Cécile Fischer[a,2,3], and Alain Perret[a,2,3]

[a]Génomique métabolique, Genoscope, Institut François Jacob, Commissariat à l'Energie Atomique et aux Energies Alternatives, CNRS, Université Evry-Val-d'Essonne/Université Paris-Saclay, 91057 Evry, France

Edited by Caroline S. Harwood, University of Washington, Seattle, WA, and approved March 30, 2018 (received for review December 22, 2017)

Trigonelline (TG; *N*-methylnicotinate) is a ubiquitous osmolyte. Although it is known that it can be degraded, the enzymes and metabolites have not been described so far. In this work, we challenged the laboratory model soil-borne, gram-negative bacterium *Acinetobacter baylyi* ADP1 (ADP1) for its ability to grow on TG and we identified a cluster of catabolic, transporter, and regulatory genes. We dissected the pathway to the level of enzymes and metabolites, and proceeded to in vitro reconstruction of the complete pathway by six purified proteins. The four enzymatic steps that lead from TG to methylamine and succinate are described, and the structures of previously undescribed metabolites are provided. Unlike many aromatic compounds that undergo hydroxylation prior to ring cleavage, the first step of TG catabolism proceeds through direct cleavage of the C5–C6 bound, catalyzed by a flavin-dependent, two-component oxygenase, which yields (*Z*)-2-((*N*-methylformamido)methylene)-5-hydroxybutyrolactone (MFMB). MFMB is then oxidized into (*E*)-2-((*N*-methylformamido) methylene) succinate (MFMS), which is split up by a hydrolase into carbon dioxide, methylamine, formic acid, and succinate semialdehyde (SSA). SSA eventually fuels up the TCA by means of an SSA dehydrogenase, assisted by a Conserved Hypothetical Protein. The cluster is conserved across marine, soil, and plant-associated bacteria. This emphasizes the role of TG as a ubiquitous nutrient for which an efficient microbial catabolic toolbox is available.

bacterial metabolism | functional genomics | LC/MS-Orbitrap | trigonelline | *N*-heterocycle degradation

Extensive and accurate bacterial genome annotation is critical for developing a comprehensive and detailed understanding of cellular physiology, and is therefore a major concern in biological research. As a result, 30–40% of genes of a typical genome remain unannotated or associated with a putative function (1, 2). In many cases, function is extrapolated from a small number of characterized proteins (3). In this context, the need for a global effort of experimental assignation, validation, or correction of function is major. Experimental work guided by bioinformatics has proved to be an invaluable tool for assigning new functions (4–7). However, investigations on catabolic pathways are still often conducted in a few model organisms and with a restricted set of nutrients. Given the vast array of natural secondary metabolites and their underrepresentation in metabolic maps, the full range of transformations afforded by bacteria is clearly underestimated. Thus, simply varying the range of organisms tested and the set of nutrients remains a useful tactic for elucidating hidden latent microbial catabolic pathways and providing access to gene function (8–10).

Trigonelline (TG; *N*-methylnicotinate) is a metabolite of nicotinamide involved in plant cell cycle regulation and oxidative stress (11). Released by legume roots and seeds, such as in alfalfa, it activates nodulation genes in *Rhizobium meliloti* (12). It is one of the most widely distributed betaines in higher plants (12, 13), and it is also present with different concentration ranges in organisms such as reef-building corals (14, 15), algae (16), and marine plankton, in which it can reach the millimolar range (17, 18). It is likely released in the environment through the death of these organisms. As a consequence, numerous heterotrophic prokaryotes probably use this compound as a nutrient. Surprisingly, the soil bacterium *R. meliloti* RCR2011 is the only organism reported to use TG as a carbon, nitrogen, and energy source (19). Although an inducible genetic region involved in the degradation of this compound was specified (20, 21), investigations aimed at deciphering this metabolic pathway did not go further. Therefore, the complete set of genes and catabolites involved in this process is not reported.

Acinetobacter baylyi ADP1 (ADP1) is a nutritionally versatile strictly aerobic bacterium capable of metabolizing a wide range of aromatic compounds (22). Its extraordinary competence for natural transformation and the ease with which it can be genetically engineered (23, 24) make ADP1 a key organism for the study of soil bacteria metabolism of natural compounds. In this work, we show that ADP1 can use TG as the sole source of carbon, nitrogen, and energy. A gene cluster responsible for TG degradation, which we called *tgn* (for trigonelline), was revealed

Significance

The experimental dissection of novel metabolic pathways, from genes and enzymes to metabolites, is a key issue for improving our knowledge of the enzymatic capabilities of the microbial world and providing accurate functional annotation of genomes. We used an integrative methodology combining the phenotyping of a complete genome-scale mutant collection of *Acinetobacter baylyi* ADP1 with an untargeted liquid chromatography/MS-based approach to uncover the degradation pathway of trigonelline (TG), a widespread osmolyte. We provide extensive information about this unusual *N*-heterocyclic aromatic degradation route that expands the metabolite repertoire. The occurrence of conserved gene clusters for TG dissimilation in soil, plant-associated, and marine bacteria underlines its environmental abundance.

Author contributions: P.-L.S., C.F., and A.P. designed research; N.P., P.-L.S., E.D., C.P., J.-L.P., M.B.-G., M.D., A.G., and C.F. performed research; V.d.B. contributed new reagents/analytic tools; N.P., P.-L.S., E.D., M.S., C.F., and A.P. analyzed data; and P.-L.S., C.F., and A.P. wrote the paper.

The authors declare no conflict of interest.

This article is a PNAS Direct Submission.

[1]N.P. and P.-L.S. contributed equally to this work.

[2]C.F. and A.P. contributed equally to this work.

[3]To whom correspondence may be addressed. Email: fischer@genoscope.cns.fr or aperret@genoscope.cns.fr.

This article contains supporting information online at www.pnas.org/lookup/suppl/doi:10.1073/pnas.1722368115/-/DCSupplemental.

Published online April 23, 2018.

by phenotypic profiling of ~2,600 strains from the ADP1 mutant strains collection (25). We investigated this metabolic route via an untargeted liquid chromatography (LC)/MS-based approach. The structure of previously undescribed catabolites was solved, and the enzymes were characterized kinetically, allowing us to provide a functional annotation of the corresponding *tgn* genes. The distribution of the *tgn* cluster in more than 200 genomes of soil, plants, and marine bacteria highlights the role of this compound as a ubiquitous nutrient.

Results

Identification of the TG Gene Cluster in ADP1. ADP1 readily grows on TG when added to a defined mineral medium as the sole nitrogen and carbon source. Growth phenotypes of the whole-mutant strains collection were investigated after 24 h in liquid *Acinetobacter* minimal medium containing TG as the sole carbon source (Fig. 1). The deletion of any gene from *ACIAD2541–ACIAD2545* abolished cell growth. ACIAD2541 is annotated as a putative purine-cytosine permease. Genes orthologous to *ACIAD2542–ACIAD2545* but also to the nearby *ACIAD2539* and *ACIAD2546* are present on a symbiotic megaplasmid in *Sinorhizobium meliloti* 1021 (*SMa0792–SMa0796*, *SMa0805*, and *SMa0791*, respectively) (Fig. 2). *S. meliloti* 1021 is a spontaneous streptomycin-resistant mutant of *R. meliloti* RCR2011 (26), the only organism reported to degrade TG (20, 21). In *R. meliloti* RCR2011, the genes involved in TG degradation were allocated near the *nif-nod* genes, 4 kb downstream of the *nifAB* genes (21), as are *SMa0791–SMa0805* in *S. meliloti* 1021. The absence of a permease gene homologous to *ACIAD2541* in *S. meliloti* 1021 is compensated for by the presence of genes of the ATP-binding cassette (ABC) transporter family (*Sma0799–Sma0803*).

We investigated the growth kinetics of mutant strains deleted for *ACIAD2539*, *ACIAD2542–ACIAD2545*, and *ACIAD2546* with TG as the carbon source, the nitrogen source, or both. While not abolished, the growth of strains deleted for *ACIAD2539* and *ACIAD2546* was indeed affected (Fig. S1), suggesting that these genes also play a role in TG degradation.

We propose to assign the name *tgn* to the genes that are responsible for TG degradation (Table 1). They all are in the same transcriptional orientation (Fig. 2), except *ACIAD2547*, which is annotated as a transcriptional regulator of the GntR family. Deletion of this gene did not affect growth on TG, as can be expected for a negative regulator. This gene cluster is flanked upstream and downstream in ADP1 by genes of the monomethylamine catabolism pathway (27), suggesting that methylamine is a final catabolite that is used as the nitrogen source. On the other hand, according to the annotation of ACIAD2539 [succinate semialdehyde (SSA) dehydrogenase], it can be anticipated that succinate is the entry point in the central metabolism.

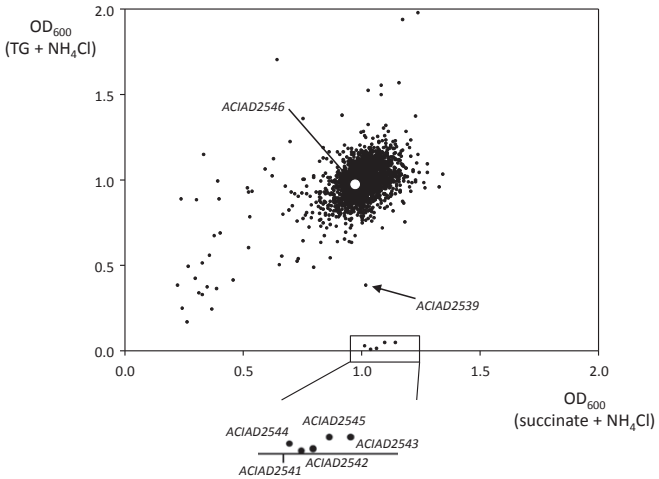

Fig. 1. Phenotyping of the genome-scale ADP1 mutant collection on TG and succinate as the carbon sources. The mineral medium was supplemented with 10 mM TG or succinate as the carbon source and 18 mM ammonium as the nitrogen source. The medium was inoculated from an overnight culture pregrown on ammonium and succinate. Cell growth from duplicate independent cultures was measured by OD_{600} after 24 h. The squared area represents mutants growing poorly on TG, while presenting significant growth on succinate plus ammonium. Annotation of genes is provided in Table 1.

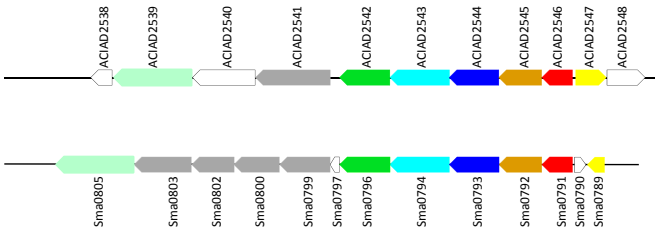

Fig. 2. TG degradation gene cluster in ADP1 and *S. meliloti* 1021. Physical colocalization of genetic loci was observed through the MicroScope platform (65). Transporter genes are all colored gray, irrespective of the transporter family. The same applies to predicted transcriptional regulators (yellow). Uncolored gene symbols are used for genes apparently unrelated to TG degradation. ACIAD, *Acinetobacter baylyi* ADP1; Sma, *Sinorhizobium meliloti* 1021.

Complete in Vitro Conversion of TG to Succinate. *ACIAD2539* and *ACIAD2542–ACIAD2546* were heterologously transcribed in *Escherichia coli*, and the corresponding proteins were purified (*SI Materials and Methods* and Fig. S2). They were incubated together in the presence of TG, FMN, and NADH (*SI Materials and Methods*) for 180 min. These cofactors were selected according to the functional annotation of ACIAD2544 on the one side (NADH FMN-dependent reductase) and that of ACIAD2539 and ACIAD2542 on the other side (NAD^+ oxidoreductases). A control mixture devoid of enzymes was incubated in the same conditions. The comparative analysis of metabolite profiles of the two reaction mixtures was conducted using the web-based platform XCMS Online (28). Results indicated the total consumption of TG (Fig. S3) and the formation of a compound identified as succinate, according to comparison of its retention time, accurate mass, and MS^2 spectra with a reference standard (Fig. S4 *A* and *B*). In the presence of the six candidate proteins, 500 μM TG was converted to succinate (536 ± 48 μM; $n = 3$). However, in the absence of TgnF, while all TG was consumed, less succinate was produced (444 ± 51 μM; $n = 3$), supporting the involvement of this Conserved Hypothetical Protein in TG catabolism.

Layout of the TG Degradation Pathway. ACIAD2544 is annotated as "putative flavin reductase." Its N-terminal domain displays 48% identity with C1-hpah from *Acinetobacter baumanii*, a reductase that supplies $FMNH_2$ to the 4-hydroxyphenylacetic acid oxygenase, and 32% identity with the RutF reductase from *E. coli* that provides the RutA oxygenase with $FMNH_2$ for opening of the pyrimidine ring of uracil (29). These two enzymatic systems are flavin-dependent, two-component monooxygenase systems (30). Wright and Cain (31) proposed that the degradation of *N*-methylisonicotinate (a TG isomer) started with an NADH-dependent enzyme, and ring opening was suggested to be the first enzymatic step in the degradation of pyridine by *Bacillus* spp. (32, 33). Since ACIAD2543 is annotated as "putative monooxygenase," we checked whether ACIAD2544 (TgnA) and ACIAD2543 (TgnB) could form a two-component monooxygenase system catalyzing the first step of the TG degradation pathway. We conducted a comparative analysis of metabolite profiles between a mixture containing TG plus NADH and FMN in the presence and absence of TgnAB, and detected an anion of

Table 1. Functions of the genes involved in TG degradation

Gene ID	Predicted function*	Function	Gene name
ACIAD2539	SSA dehydrogenase	SSA dehydrogenase†	*tgnE*
ACIAD2541	Putative purine-cytosine permease	TG permease†	*tgnP*
ACIAD2542	Putative aldehyde dehydrogenase	MFMB dehydrogenase†	*tgnC*
ACIAD2543	Putative monooxygenase	TG oxygenase†,‡	*tgnB*
ACIAD2544	Putative flavin reductase	TG oxygenase†,§	*tgnA*
ACIAD2545	Putative hydrolase	MFMS hydrolase†	*tgnD*
ACIAD2546	Conserved Hypothetical Protein (CHP)	SSA dehydrogenase stimulating protein†	*tgnF*
ACIAD2547	Transcriptional regulator (GntR family)	TG degradation transcriptional regulator	*tgnR*

*Based on genome annotations.
†Experimental evidence from this work.
‡Oxygenase component.
§Reductase component.

m/z = 170.045 (catabolite A; $C_7H_8NO_4$), while the peak for TG decreased (Fig. 3 *A* and *B*). To identify the next enzyme in the pathway, we added a third enzyme to a reaction mixture containing TG and TgnAB, and observed that the peak of m/z = 170.045 decreased only in the presence of ACIAD2542 (TgnC). Concomitantly, another anion (catabolite B; m/z = 186.040) was produced (Fig. 3*C*). ACIAD2545 (TgnD) is the fourth enzyme, since when added in a mixture with TgnAB and TgnC, SSA was produced (Fig. 3*D*). The identity of SSA was confirmed by comparing its accurate mass, MS^2 spectra, and retention time with a reference compound (Fig. S4 *C* and *D*). Finally, with the addition of ACIAD2539 (TgnE, annotated as SSA dehydrogenase), SSA was converted to succinate (Fig. 3*E*). However, in these conditions, some SSA remained in the mixture, while upon addition of TgnF, SSA was no longer detectable and the peak height of succinate increased (Fig. 3*F*), suggesting that TgnF participates in SSA oxidation. This is in agreement with our material balance analysis experiments for the whole pathway mentioned above, which showed that a 1:1 conversion ratio of TG into succinate was obtained only in the presence of TgnF. It is also consistent with the observed growth delay for the strain deleted for *ACIAD2546* (Fig. S1). While not strictly required for the in vitro catabolism of TG, TgnF nevertheless stimulates the conversion rate of SSA to succinate.

Two Previously Unreported Metabolites Are Produced During TG Catabolism. The products of TgnAB and TgnC, detected as anions of m/z = 170.045 and m/z = 186.040, respectively, were both synthesized on a 10-mg scale starting from TG and a combination of TgnAB and TgnABC (*SI Materials and Methods*). Their structures were elucidated using a series of 1D and 2D NMR experiments (Fig. 4 *A*–*D* and Dataset S1). The product of TgnAB (catabolite A) is a cyclic compound with a butyrolactone ring, (*Z*)-2-((*N*-methylformamido)methylene)-5-hydroxy-butyrolactone (MFMB),

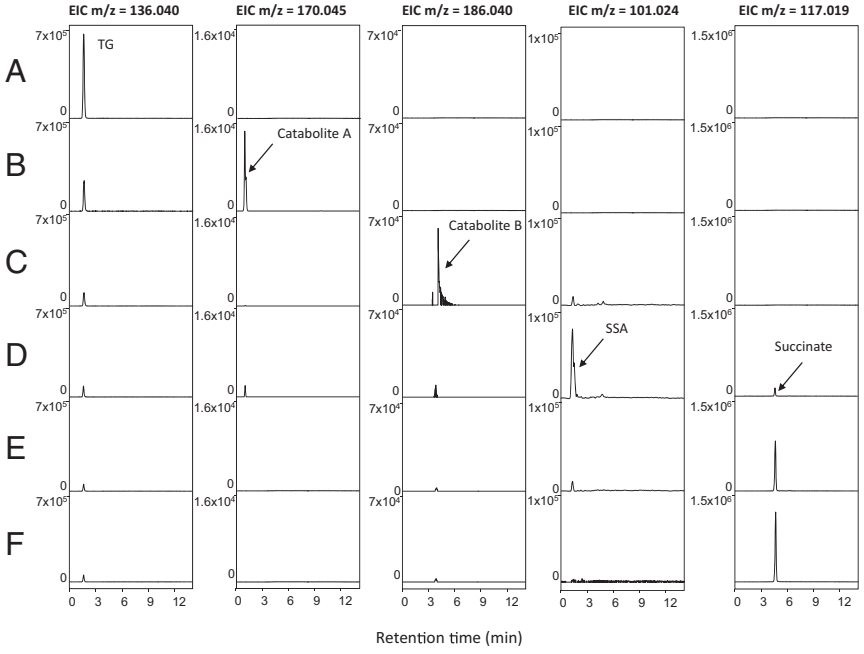

Fig. 3. In vitro reconstruction of the TG degradation pathway. The initial substrate concentrations were 500 μM TG, 1.5 mM NADH, and 25 μM FMN in a final volume of 100 μL. Two micrograms of each protein was added. (*A*) Sample of the reaction mixture in the absence of enzyme. (*B*) Sample analyzed 30 min after addition of TgnA and TgnB. (*C*) Sample analyzed 30 min after addition of TgnAB and TgnC. (*D*) Sample analyzed 30 min after addition of TgnAB, TgnC, and TgnD. (*E*) Sample analyzed 30 min after addition of TgnAB, TgnC, TgnD, and TgnE. (*F*) Sample analyzed 30 min after addition of TgnAB, TgnC, TgnD, TgnE, and TgnF. Samples were analyzed by LC/MS in the negative ionization mode. The extracted ion chromatograms (EICs) correspond to the quasimolecular ions ($[M-H]^-$) of TG [m/z = 136.040 atomic mass units (amu)], catabolite A (m/z = 170.045 amu), catabolite B (m/z = 186.040 amu), SSA (m/z = 101.024 amu), and succinate (m/z = 117.019 amu) at 5 ppm accuracy.

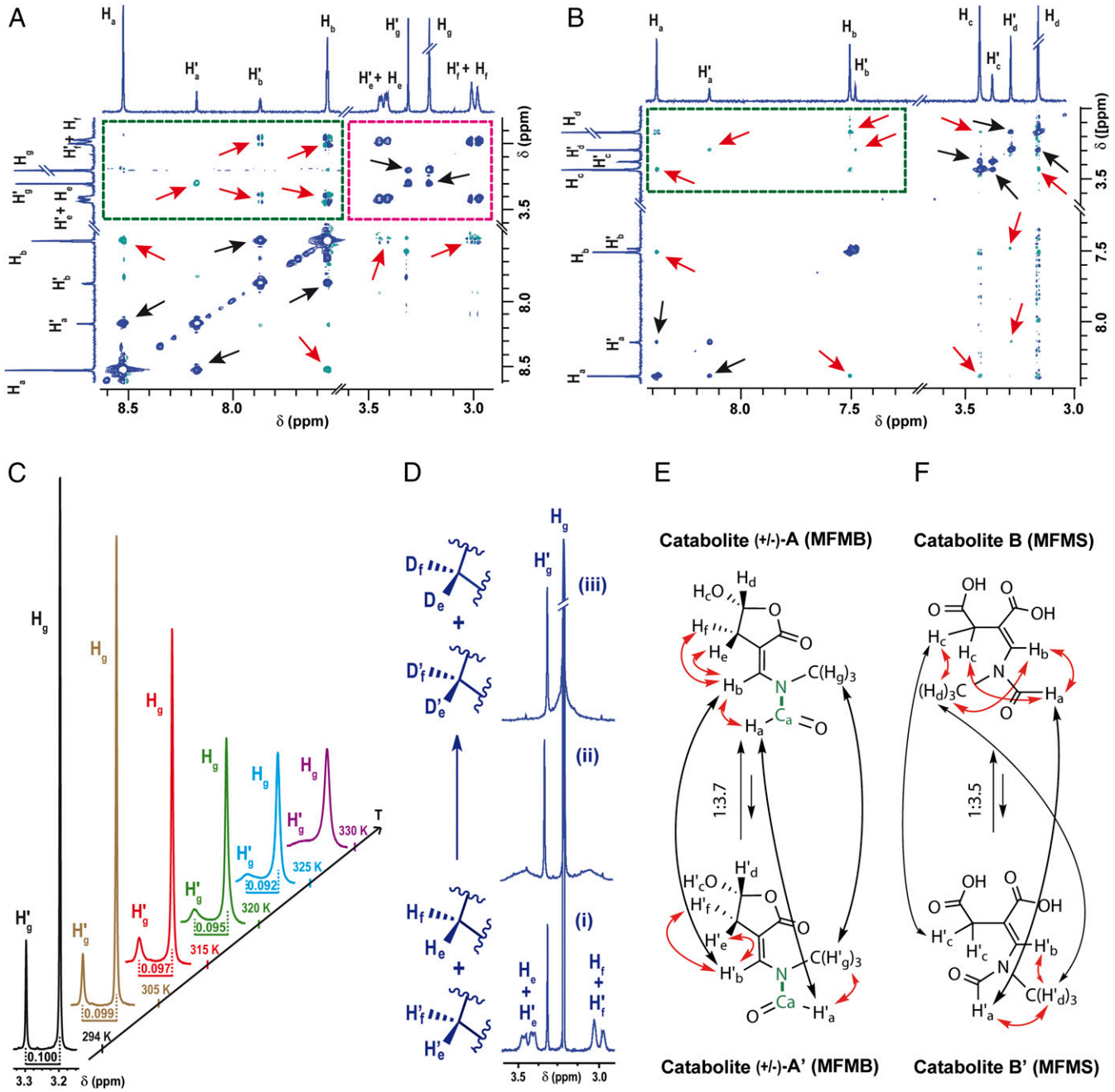

Fig. 4. Structural elucidation of MFMB and MFMS. ^{1}H-^{1}H ROESY experiments (600 MHz) at 298 K for MFMB [conformers (+/–)-A and (+/–)-A′ in equilibrium] (*A*) and MFMS [conformers (+/–)-B and (+/–)-B′ in equilibrium] (*B*) in D_2O. Most significant chemical exchange correlations and NOE correlations are pointed to on both ROESY spectra and the respective catabolite structures (*E* and *F*) with black and red arrows. Chemical exchange correlations demonstrate conformational equilibria (e.g., correlation between H_a and H′$_a$ indicates that H_a becomes H′$_a$ during the NMR experiment time scale). The intensity of NOE correlations is related to the spatial distance between protons belonging to the same molecule, and it allows the determination of the C = C bond configuration in MFMB and MFMS catabolites, as well as the 3D conformation of all catabolite isomers. For clarity, several signal intensity levels were combined together: (*i*) medium level for the general ROESY frames, (*ii*) high level in green dashed boxes, and (*iii*) low level in pink dashed box. ROESY original spectra for each intensity level are provided in Dataset S1 *A–E*. (*C*) *N*-methyl region from ^{1}H NMR spectra (600 MHz) of MFMB at different temperatures in CD_3CN illustrates the dynamic equilibrium between rotamers. Rotation around the N-C_a bond interconverts the position of the formyl group, and hence modifies the chemical environment of the *N*-methyl protons H_g and H′$_g$ (*E*, in green). At 294 K, when this interconversion is too slow compared with the ^{1}H NMR acquisition time scale, the ^{1}H spectrum of the *N*-methyl groups consists of two sharp peaks arising from H_g and H′$_g$. As the temperature is increased and the rate of interconversion becomes faster, the peaks broaden and tend to merge. The same phenomenon occurs for formyl (H_a and H′$_a$) and vinyl (H_b and H′$_b$) protons as well (Fig. S5*A*). (*D*) Slow proton/deuterium exchanges within MFMB rotamers are evidenced by the disappearance of the H_e + H′$_e$ and H_g + H′$_g$ signals of MFMB in $CDCN_3$ (i) upon addition of D_2O to the $CDCN_3$ sample (ii) and subsequent redissolution in $CDCN_3$ of the lyophilizate (iii). These exchanges indicate that H_e + H′$_e$ and H_g + H′$_g$ are enolizable protons in the α-position of the aldehyde group of open isomers (even at a neutral pH), which are in equilibrium with closed structures. (*E* and *F*) Structures of MFMB and MFMS conformers, respectively, as inferred from their NMR data.

which turned out to be a 3.7:1 mixture of two amide conformers, (+/−)-A and (+/−)-A′ in CD_3CN (Fig. 4 *A* and *E*). Additional analyses highlighted more in depth the dynamic structure of MFMB: Chemical exchange correlations in a rotating-frame nuclear overhauser effect correlation spectroscopy (ROESY) NMR experiment were observed between protons of A and A′ (Fig. 4*A*). The presence of such dynamic equilibrium between the two conformers was confirmed by studying the effect of the temperature on the signal of several sets of protons [*N*-methyl groups (Fig. 4*C*), formyl and vinyl protons (Fig. S5*A*)]. The 3.7:1 ratio was not affected by replacing CD_3CN with D_2O; however, a slow proton/deuterium exchange was observed for methylene protons (Fig. 4*D*). It demonstrated the occurrence of an additional aldehyde-hemiacetal equilibrium involving two NMR-invisible (i.e., quantitatively marginal) 4-oxobutyrate open forms that could tautomerize and incorporate deuterium atoms (Fig. S5*B*). Conversely, the product of TgnC (catabolite B), ((*E*)-2-((*N*-methylformamido)methylene)succinate (MFMS), appeared in D_2O as a simple 3.5:1 mixture of two exchangeable alicyclic conformers (B and B′; Fig. 4*F*) as revealed by chemical exchange correlations in ROESY NMR spectrum (Fig. 4*B*). Unexpectedly, an inversion of the C = C bond stereochemistry was observed when MFMB was oxidized into MFMS (Fig. 4 *E* and *F*). This probably originates from the rare exoenamide moiety, which may be prone to isomerization (34).

TgnAB Is an Allosteric Two-Component, Flavin-Dependent TG Oxygenase. Reductases of these systems are usually classified by their flavin dependence (30). TgnA was purified as a homodimer, according to gel filtration experiments, and the concentrated protein was indeed slightly yellow, indicating the presence of a cofactor. LC/MS analysis and quantitation showed that only 10% of purified TgnA was complexed to a cofactor. However, both FAD and FMN were released from purified TgnA upon heat denaturation, with FAD accounting for 44% of the bound cofactors (Fig. S6). The recombinant enzyme is thus a mixture of polypeptides that have bound either FAD or FMN. Upon dilution for enzymatic characterization, NADH oxidation by TgnA was not detected in the absence of added flavin (Fig. 5 *E* and *G*). This reflected the fact that flavin acts as a substrate and is not a prosthetic group, as reported by Ellis (30). TgnA exhibited TG-stimulated NADH (but not NADPH) oxidation. Kinetics of NADH oxidation performed at fixed concentrations of TG and FMN with variable NADH concentrations were hyperbolic (Fig. 5 *A* and *B* and Table 2). Conversely, kinetics conducted at variable TG concentrations were sigmoidal (Fig. 5 *C* and *D* and Table 2). The cooperative behavior is illustrated by nonlinearity in the Eadie–Hofstee representation (v versus $v/[S]$ where v represents the initial rate of NADH oxidation and $[S]$ the substrate concentration) in Fig. 5*D*. TgnA could therefore undergo an allosteric transition upon TG binding accounting for the positive cooperativity toward NADH oxidation, a behavior similar to the one described for C1-hpah of *A. baumanii* (35). TgnA contains an extra C-terminal domain like the reductases from *A. baumanii* (35) and *Chelatobacter* strain ATCC 29600 (36), which are involved in the monooxygenation of hydroxyphenylacetate and nitrilotriacetate, respectively. To investigate further the role of the TgnA C-terminal domain, we constructed a truncated TgnA containing only residues 1–161 (TgnA-Nter). The rate of NADH oxidation of TgnA-Nter measured at a saturating nucleotide concentration (300 μM) was similar to the one observed for the wild-type enzyme in the presence of saturating concentrations of both TG and NADH, showing that TG could no longer influence NADH oxidation by TgnA-Nter. The C-terminal domain therefore seems to be responsible for TG binding and allosteric stimulation of flavin reduction by NADH. As reported for *A. baumanii* C1-hpah (37), the C-terminal region acts as an inhibitory domain for the N-terminal reductase domain.

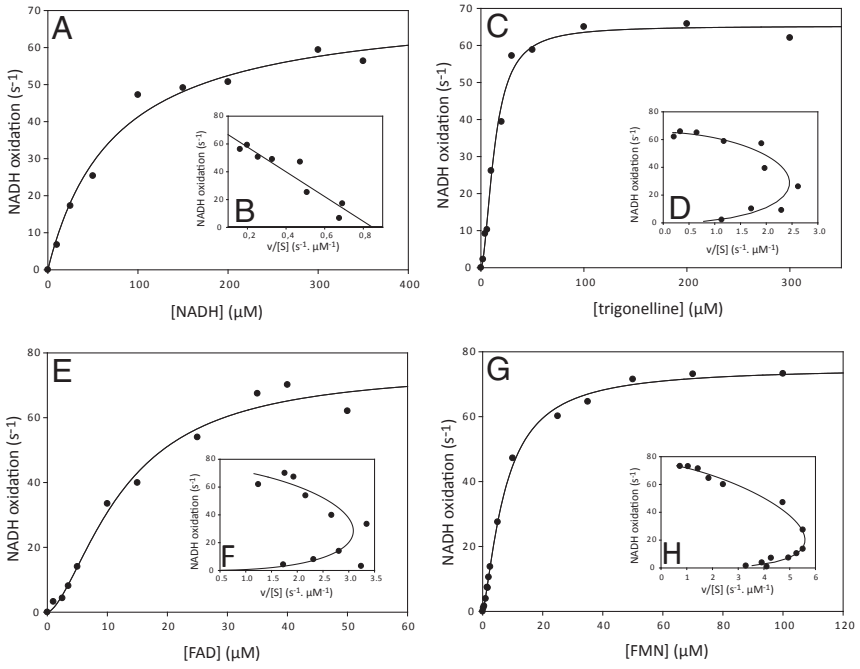

Fig. 5. Steady-state kinetics of NADH oxidation by TgnA in the presence of TG. (*A* and *B*) Rates of NADH oxidation versus NADH concentration in the presence of saturating concentrations of TG and FMN. (*C* and *D*) Rates of NADH oxidation versus TG concentration in the presence of saturating concentrations of NADH and FMN. (*E* and *F*) Rates of NADH oxidation versus FAD concentration in the presence of saturating concentrations of TG and NADH. (*G* and *H*) Rates of NADH oxidation versus FMN concentration in the presence of saturating concentrations of TG and NADH. v, the initial rate of the reaction, is expressed in moles of NADH oxidized per second and per mole of enzyme. Curves were drawn using Sigma-Plot software. The Michaelis–Menten equation $v = (V_{max}\,S)/(K_m + S)$ applies for plot *A*, and the Hill equation $v = (V_{max}\,S^n)/(S_{50}{}^n + S^n)$ applies for plots *C*, *E*, and *G*. S_{50} is the substrate concentration showing half-maximal velocity, n is the Hill coefficient, and V_{max} is the maximal velocity. (*B*, *D*, *F*, and *H*) Eadie–Hofstee representation (v versus v/S) of the kinetics.

Table 2. Kinetic parameters for TgnA

	Michaelian parameters			Non-Michaelian parameters		
Substrate	K_m, μM	k_{cat}, s^{-1}	k_{cat}/K_m, $s^{-1}\cdot M^{-1}$	S_{50}, μM	V_{max}, s^{-1}	n
NADH*	74 ± 14	72 ± 4	9.7×10^5			
TG†				13 ± 1	65 ± 2	1.80 ± 0.2
FMN‡				8 ± 1	75 ± 1	1.36 ± 0.1
FAD‡				13 ± 2	75 ± 7	1.61 ± 0.3

*TG and FMN concentrations were 300 μM and 80 μM, respectively.
†NADH and FMN concentrations were 300 μM and 80 μM, respectively.
‡TG and NADH concentrations were 300 μM each. Values correspond to the average of two replicates.

Considering FAD and FMN as substrates, we studied saturation for FAD (Fig. 5 *E* and *F*) and FMN (Fig. 5 *G* and *H*) by monitoring NADH oxidation with various flavin concentrations in the presence of saturating concentrations of NADH and TG. NADH oxidation was detected in the presence of both flavins. Kinetics with increasing flavin concentrations were sigmoidal for both FAD and FMN. Kinetic parameters (Table 2) show that V_{max} on one side (75 s^{-1} for FAD or FMN) and S_{50} on the other side (13 μM and 8 μM for FAD and FMN, respectively) are similar, demonstrating that TgnA is as efficient with FAD as with FMN. The observed cooperativity suggests that binding of one molecule of flavin to one of the subunits of the dimer affects further binding to the second one. Such a behavior was reported for D-amino acid oxidase and FAD (38). TgnB was purified as a homodimer. Its enzymatic activity was investigated in the presence of TgnA. TgnB is annotated as a putative monooxygenase, but the comparison of the elemental composition in negative ionization mode of its substrate (TG; $C_7H_6NO_2$) and product (MFMB; $C_7H_8NO_4$) suggests a dihydroxylase activity instead.

Flavin transfer in two-component system oxygenases can occur via simple flavin diffusion (39, 40) or complex formation (41, 42). We investigated the interaction between TgnA and TgnB by size-exclusion chromatography. TgnA and TgnB were first analyzed alone and eluted at 30 min and 29 min, respectively. Elution time was unchanged when TgnA and TgnB were coinjected (in the presence and absence of TG), indicating that they do not form a stable complex for flavin transfer.

So far, the oxygenases of two-component systems have been classified by the flavin used (30, 43–47). We observed formation of MFMB by TgnB in the presence of FAD or FMN, in agreement with the versatility of TgnA regarding flavin usage (MFMB formation was detected by LC/MS in the presence of FMN, while it was enzymatically produced for structural characterization with FAD). In sum, the initial step of TG degradation is catalyzed by two enzymes (Fig. S7). TgnA supplies a reduced flavin to TgnB, which binds the reduced flavin and activates molecular oxygen to catalyze TG oxidation. NADH oxidation and TG oxygenation are catalyzed by distinct enzymes, and the flavin transfer process from TgnA to TgnB may simply be under thermodynamic control (45).

TgnC Is an MFMB Dehydrogenase. TgnC was purified as a homodimer. It is annotated as "putative aldehyde dehydrogenase" and was evaluated in converting MFMB to MFMS. Its activity, first established by LC/MS analysis, was further studied spectrophotometrically by monitoring the kinetics of NAD^+ reduction (Table 3) since it is almost inactive with $NADP^+$ (below 0.1% activity compared with NAD^+). This is consistent with the presence of a proline at position 181 (48).

TgnD Is an MFMS Hydrolase. ACIAD2545 (TgnD) was purified as a monomer. The enzyme shares 23% identity with 2-(acetamidomethylene) succinate (ACMS) hydrolase from *Mesorhizobium loti* MAFF303099, which is involved in the pyridoxine degradation pathway. It converts ACMS to SSA, acetate, carbon dioxide, and ammonia (49). Considering, on the one hand, that methylamine is a plausible final catabolite and, on the other hand, a mechanistic similarity between ACMS hydrolase and TgnD, the latter should yield SSA (discussed above), methylamine, formate, and carbon dioxide. Methylamine and formate were actually detected in a mixture containing TG, TgnAB, TgnC, and TgnD but could not be detected in the absence of TgnD. Similarly, these two compounds were also detected in a mixture containing purified MFMS and TgnD (*SI Materials and Methods*). The kinetic behavior of TgnD was monitored following the consumption of MFMS at 253 nm (*SI Materials and Methods*), and kinetic parameters were obtained from the concentration dependence of the rate of depletion of MFMS at a fixed concentration of enzyme (Table 3).

TgnE Is an SSA Dehydrogenase. ACIAD2539 (TgnE) was purified as a tetramer. TgnE is annotated as "SSA dehydrogenase" as are at least two other cognate SSA dehydrogenases (ACIAD0960 and ACIAD3445) in the genome of ADP1. This probably explains why the *tgnE* deletion mutant (Δ*ACIAD2539*) is able to grow (albeit slowly) in the presence of TG as a carbon source (Fig. 1 and Fig. S1). TgnE yields succinate from SSA and NAD^+. As reported for TgnC, the presence of a proline residue at position 181 indicates it is an NAD^+-preferring enzyme. TgnE activity, too, is hardly detectable with $NADP^+$ (below 1% activity compared with NAD^+), and enzyme activity was therefore followed by monitoring the formation of NADH (Table 3).

TgnF Stimulates TgnE-Dependent SSA Oxidation. ACIAD2546 (TgnF) was purified as a hexamer, in agreement with the first representatives of this Pfam family (PF06684; formerly DUF1185) (50). PF06684 contains nearly 500 sequence homologs, mostly found in Proteobacteria and Actinobacteria. We investigated the role of TgnF in stimulating succinate formation since the inclusion of TgnF in the one-pot mixture of enzymes, cofactors, and TG increased succinate yield at the expense of SSA. We could not observe any effect of TgnF alone in converting SSA in succinate. Similarly, the TgnE-dependent rate of NAD^+ reduction with fixed SSA concentrations was not enhanced in the presence of TgnF. However, a stimulating effect of TgnF on TgnE was observed when SSA was continuously produced from MFMS and TgnD. Therefore, the influence of the concentration of TgnF on SSA oxidation at a constant concentration of TgnE was investigated (Fig. S8). The catalytic activity of TgnE increased hyperbolically with an increasing concentration of TgnF, with a half-saturation value of 0.7 ± 0.3 molecule of TgnF per molecule of TgnE. These data are in agreement with the formation of a complex between TgnE and TgnF. We thus hypothesized that TgnE and TgnF could form a complex, together with TgnD, to convert the reactive SSA as soon as it is produced. We investigated their interaction by size-exclusion chromatography. The proteins were first analyzed individually and then

Table 3. Kinetic parameters for TgnE, TgnC, and TgnD

Enzyme	Substrate	K_m, μM	k_{cat}, s^{-1}	k_{cat}/K_m, $s^{-1}\cdot M^{-1}$
TgnE	NAD^+*	107 ± 8	61.5 ± 6.8	5.7×10^5
	SSA†	72 ± 11		8.5×10^5
TgnC	NAD^+‡	900 ± 190	2.5 ± 0.4	2.8×10^3
	MFMB§	140 ± 40		1.8×10^4
TgnD	MFMS	222 ± 50	112.3 ± 11.1	5.0×10^5

*SSA concentration was 250 μM.
†NAD^+ concentration was 5 mM.
‡MFMB concentration was 1.3 mM.
§NAD^+ concentration was 6.6 mM. Values correspond to the average of two replicates.

BIOCHEMISTRY

injected together at a TgnF/TgnE/TgnD molar ratio of 4:1:1 in the presence and absence of 500 μM SSA. A complex was not observed, since the elution time of the proteins remained unchanged. We then considered Colorless-Native PAGE but could not visualize any complex. Based on these observations, we assume that the proteins are only weakly associated and do not form a stable complex.

The Aerobic TG Degradation Pathway. Based on these results, we propose the catabolic pathway for TG in ADP1 (Fig. 6). TG is first oxygenized to MFMB by the two-component, flavin-dependent oxygenase TgnAB. MFMB is then oxidized in MFMS by the MFMB dehydrogenase TgnC, and hydrolyzed to carbon dioxide, formate, methylamine, and SSA by the MFMS hydrolase TgnD. SSA is eventually oxidized in succinate by TgnE, stimulated by TgnF.

Discussion

The data presented here indicate that ADP1 degrades the pyridine ring of TG in succinate and methylamine as carbon and nitrogen sources, respectively, using an undescribed catabolic pathway. Comparative analyses conducted on the MicroScope platform (https://www.genoscope.cns.fr/agc/microscope/home/index.php) showed that clusters of genes orthologous to *tgnA–tgnF* (*tgnE* can be located elsewhere in the genome) are present in the chromosome of more than 200 organisms (as of October 2017). Most clusters harbor genes for a GntR-type transcriptional regulator and transporter(s). Although distributed in four taxonomic classes (α-, β-, and γ-Proteobacteria and Actinobacteria), the *tgn* cluster is mainly encountered in Proteobacteria. Its presence in the gram-positive Actinobacteria suggests lateral gene transfer events during evolution. Surprisingly, Actinobacteria have two homologous *tgnF* genes repeated in tandem (Fig. 7). Also, in some clusters, the candidate gene for TgnA codes only for the N-terminal domain (the reductive part, without the regulatory domain). The *tgn* cluster is logically anticipated in organisms that encounter TG in their habitat. Plants are a major source of TG, and *tgn* genes are accordingly observed in bacteria that interact with them (*Sinorhizobium*, *Agrobacterium*, and *Azospirillum*) or in soil organisms (*Burkholderia*, *Pseudomonas*, *Acinetobacter*, and *Saccharopolyspora*). Additionally, since TG is present in the marine environment, the *tgn* cluster is found in genera like *Marinomonas*, *Pseudovibrio*, *Pelagibacter*, and *Streptomyces*.

Despite structural similarities between TG (*N*-methylnicotinate) and nicotinate, this pathway is dedicated to TG, as nicotinate is not metabolized by ADP1. Three different pathways have been reported for the degradation of nicotinate in different organisms (51). Two similar pathways lead to fumarate. In the third one, nicotinate is degraded into acetyl-CoA. Nevertheless, these three pathways have in common the first enzymatic step that hydroxylates nicotinate into 6-hydroxynicotinate. TG is degraded completely differently. Interestingly, *Pseudomonas putida* KT2440 degrades nicotinate (52) and contains the cluster for TG degradation. We could observe that it readily grows on TG. Thus, this organism uses totally different pathways to metabolize related compounds.

The building up of a metabolic pathway could be considered as the trade-off between different constraints, such as thermodynamics and chemical reactivity (53, 54). This reactivity can lead a molecule to be transformed by different chemical reactions. As an illustration, the first step in the catabolic pathways of the *N*-heterocycles pyridine, pyridoxine, and *N*-methylisonicotinate can each begin with different chemical reactions according to the degrading organism (51, 55). In other words, the reactions of a metabolic pathway in an organism can also be driven by the nature of the ancestral proteins that have evolved to create new enzyme functions (56, 57). Gene shuffling and transfer shape the gene content, and thus the metabolic abilities of an organism. One can think that the nicotinate and TG degradation pathways were created independently, using distinct chemical transformations, and that these pathways are eventually found in the same organism by lateral gene transfer. However, it can be argued that a TG-demethylating activity followed by a nicotinate pathway could be also a plausible alternative metabolic solution. Whether it exists in some bacteria would deserve attention.

N-heteroaromatic compounds are known to be utilized by bacteria as carbon, nitrogen, and energy sources. The aerobic degradation of these substrates usually involves the formation of hydroxylated metabolites that can be detected and their subsequent ring opening by a dioxygenase. Here, the deconstruction of TG proceeds through a different catalytic scheme. A single enzyme, TgnB, formally catalyzes the insertion of two oxygen and hydrogen atoms, followed by a ring cleavage in a reaction

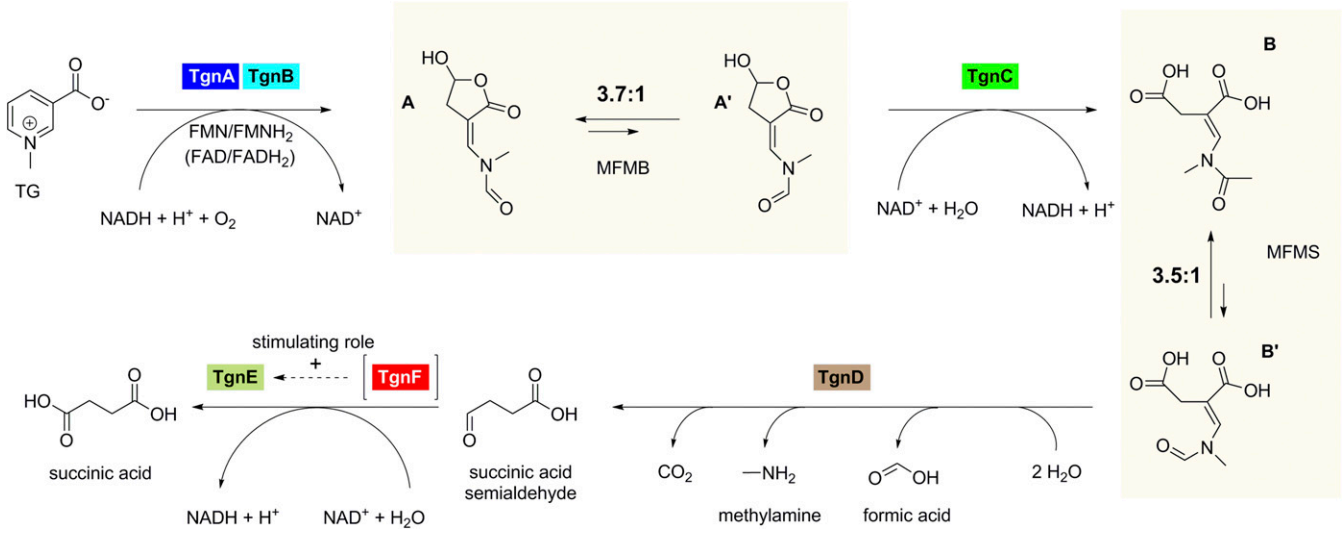

Fig. 6. TG degradation pathway in ADP1. TgnA and TgnB, two-component TG oxygenase; TgnC, MFMB dehydrogenase; TgnD, MFMS hydrolase; TgnE, SSA dehydrogenase; TgnF, SSA dehydrogenase-stimulating protein. Data from NMR analysis for MFMB and MFMS are indicated in gray boxes. A and A′ represent the two closed-form conformers of MFMB detected by NMR. B and B′ represent the two conformers of MFMS. TgnF is indicated in brackets since it is not known whether it is an enzyme.

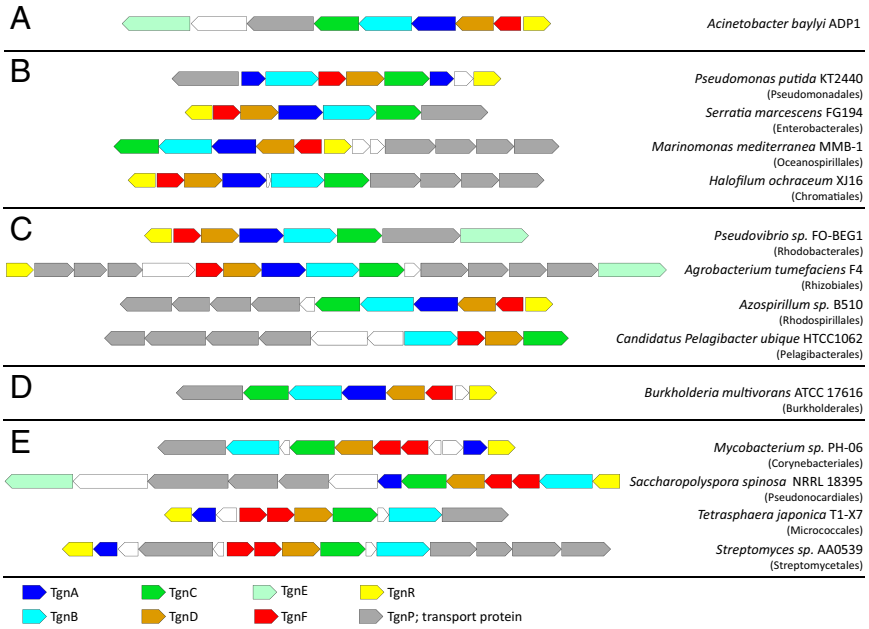

Fig. 7. Illustration of the taxonomic diversity of homologous predicted TG-degradation gene clusters. Homologous gene clusters in bacterial genomes were retrieved using MicroScope. Shown are gene clusters that contain homologous genes to ADP1 (*A*) for at least four of the six catalytic proteins of the TG-degradation pathway in γ-, α- and β-Proteobacteria (*B–D*, respectively) and in Actinobacteria (*E*). Taxonomic orders are indicated in brackets. Candidate genes for transporters and transcriptional regulators were frequently found to be conserved within these clusters. Genes indicated in white are not predicted to be related to TG degradation.

evocative of the oxygenation of 2-methyl-3-hydroxypyridine-5-carboxylic acid (MHPC) by MHPC oxygenase (MHPCO) in the pyridoxine degradation pathway (58). MHPCO is a monooxygenase that formally incorporates two oxygen atoms (one comes from dioxygen and the other from the solvent). It is a FAD containing flavoprotein (with no homology with TgnB) that only binds the pyridinium form of MHPC (59). MHPCO can also use the substrate analog *N*-methyl-5-hydroxynicotinic acid, where the N-atom is always positively charged. With both substrates, MHPCO leads to an oxidative aromatic ring-cleavage reaction (58). These observations may be related to TG, which always carries a positive charge on the N-atom of its pyridine ring. Similarly, in the metabolism of *N*-methylisonicotinate by an *Achromobacter* strain, a direct oxidative cleavage of the pyridinium ring was considered since no hydroxylated intermediate was detected (60). It can be assumed that the positive charge on the nitrogen atom in these pyridinium compounds renders unstable any oxidative intermediate, and thus leads to a direct cleavage. To conclude, since TgnB seems to behave as MHPCO and belongs to Pfam family PF00296 ("bacterial luciferase") that, up to now, only contains bona fide monooxygenases (30), it may represent a novel clade within family PF00296.

TgnF (ACIAD2546) is annotated as a Conserved Hypothetical Protein and belongs to Pfam family PF06684 (formerly DUF1185). Two representatives of this family, BB2672 and SPO0826 from *Bordetella bronchiseptica* and *Silicibacter pomeroyi*, respectively, were crystalized and have the *Bacillus* chorismate mutase-like fold. It was proposed on the sole basis of their structure and genomic context that these proteins have a role in amino acid synthesis (50). Here, we showed that TgnF is involved in the stoichiometric conversion of TG to succinate and, more specifically, that it stimulates up to 10-fold the activity of the SSA dehydrogenase TgnE. Moreover, Mlr6789 is another representative of the PF06684 family found in the genomic context of the pyridoxine degradation pathway in *M. loti* MAFF303099. In this pathway, 2-(acetamidomethylene)succinate is hydrolyzed by ACMS hydrolase (Mlr6787) to acetate, carbon dioxide, ammonia, and SSA in a reaction similar to that catalyzed by the TgnD hydrolase. It is noteworthy that an SSA dehydrogenase coding gene is found in the genome of *M. loti*, outside the pyridoxine degradation region. Thus, the TG degradation pathway parallels the pyridoxine pathway. In both routes, a monooxygenase proceeds to direct ring cleavage by inserting two oxygen atoms and a hydrolase breaks down its substrate in different compounds, which include SSA. Finally, a member of Pfam family PF06684 is expected to speed up the oxidation of SSA into succinate. We thus anticipate Mlr6789 also to have a role in succinate formation. On the basis of these observations, we propose that members of the PF06684 family participate in SSA oxidation.

In conclusion, our strategy based on growth profiling and untargeted LC/MS led us to decipher a catabolic pathway. This method could be applied to any catabolic pathway in any bacterium for which a genome-scale knockout mutant collection is available, such as *E. coli* (61), *Bacillus subtilis* (62) or *Pseudomonas aeruginosa* (63). In the absence of such a collection, this strategy could nevertheless be transposed to gene clusters selected by alternative means. For instance, the genes involved in nicotinate degradation in *P. putida* were spotted by in silico analysis (52). Those that degrade sulfoquinovose in *E. coli* were detected by proteomics (64). In the same organism, the operon that constitutes a previously undescribed pyrimidine degradation was highlighted by microarray analysis (29). In each case, gene function probably could have been assigned by the untargeted LC/MS method presented here. This strategy provided experimental evidence that five enzymes (TgnAB, TgnC, TgnD, and TgnE) are sequentially intervening in the conversion of TG to methylamine and succinate. The structures of previously undescribed metabolites were solved. We underlined the enzymatic properties of an unusual flavin-dependent, two-component oxygenase system (TgnAB) and stressed the role of one additional protein (TgnF) that enhances SSA oxidation. The probable occurrence of this metabolic route in numerous organisms of different taxa is consistent with the abundance of TG in the

environment. This natural product, along with other N-containing compatible solutes, could make a significant contribution to ecosystem nitrogen and carbon cycling.

Materials and Methods

A detailed version of the material and methods used in this study can be found in *SI Materials and Methods*. Recording the growth phenotypes of ADP1 strains, construction of expression plasmids and purification of recombinant proteins were performed using standard procedures. NADH consumption, formate or methylamine production, and MFMS consumption in enzymatic reactions were assessed spectrophotometrically using a Safas UV mc^2 double-beam spectrophotometer. Kinetic parameters were determined by nonlinear analysis of initial rates using SigmaPlot version 9.0 (Systat Software). LC/MS profiling of the TG degradation pathway was performed with a pool of purified candidate enzymes. High-resolution measurements were obtained with an Orbitrap Elite mass spectrometer (Thermo Fisher Scientific) fitted with a heated electrospray ionization source operating in positive and negative ionization modes. HPLC separations were conducted using an UltiMate 3000 system (Thermo Fisher Scientific) utilizing a hydrophilic column. Enzymatic production and purification of the metabolites MFMB and MFMS were performed on a semipreparative scale. MFMB was obtained after preparative TLC separation. MFMS was obtained after preparative hydrophilic interaction LC. NMR spectra were recorded on either a Bruker 300 MHz spectrometer or a Bruker Avance 600 MHz NMR spectrometer equipped with a cryoprobe (Université Evry-Val-d'Essonne/Université Paris-Saclay).

ACKNOWLEDGMENTS. We thank Olek Maciejak and Marie-Jeanne Clément-Lai Cheong from the NMR facility at the Université Evry-Val-d'Essonne/Université Paris-Saclay. We are grateful to Luis Coronel and Tatyana Kylosova, who were involved in the project as part of a student internship. We thank Corinne Cruaud for sequencing the recombinant constructions. This work was supported by grants from the Commissariat à l'Energie Atomique et aux Energies Alternatives, CNRS, and Université Evry-Val-d'Essonne/Université Paris-Saclay.

1. Galperin MY, Koonin EV (2004) 'Conserved hypothetical' proteins: Prioritization of targets for experimental study. *Nucleic Acids Res* 32:5452–5463.
2. Chang YC, et al. (2016) COMBREX-DB: An experiment centered database of protein function: Knowledge, predictions and knowledge gaps. *Nucleic Acids Res* 44: D330–D335.
3. Schnoes AM, Brown SD, Dodevski I, Babbitt PC (2009) Annotation error in public databases: Misannotation of molecular function in enzyme superfamilies. *PLoS Comput Biol* 5:e1000605.
4. Bastard K, et al. (2017) Parallel evolution of non-homologous isofunctional enzymes in methionine biosynthesis. *Nat Chem Biol* 13:858–866.
5. Erb TJ, et al. (2012) A RubisCO-like protein links SAM metabolism with isoprenoid biosynthesis. *Nat Chem Biol* 8:926–932.
6. Huang H, et al. (2015) A general strategy for the discovery of metabolic pathways: d-threitol, l-threitol, and erythritol utilization in Mycobacterium smegmatis. *J Am Chem Soc* 137:14570–14573, and erratum (2016) 138:4267.
7. Zhang X, et al. (2016) Assignment of function to a domain of unknown function: DUF1537 is a new kinase family in catabolic pathways for acid sugars. *Proc Natl Acad Sci USA* 113:E4161–E4169.
8. Bochner BR (2009) Global phenotypic characterization of bacteria. *FEMS Microbiol Rev* 33:191–205.
9. Felux AK, Spiteller D, Klebensberger J, Schleheck D (2015) Entner-Doudoroff pathway for sulfoquinovose degradation in Pseudomonas putida SQ1. *Proc Natl Acad Sci USA* 112:E4298–E4305.
10. Nichols RJ, et al. (2011) Phenotypic landscape of a bacterial cell. *Cell* 144:143–156.
11. Minorsky PV (2002) The hot and the classic. *Plant Physiol* 128:1167–1168.
12. Phillips DA, Joseph CM, Maxwell CA (1992) Trigonelline and stachydrine released from alfalfa seeds activate NodD2 protein in Rhizobium meliloti. *Plant Physiol* 99: 1526–1531.
13. Ashihara H (2008) Trigonelline (N-methylnicotinic acid) biosynthesis and its biological role in plants. *Nat Prod Commun* 3:1423–1428.
14. Hill RW, Li C, Jones AD, Gunn JP, Frade PR (2010) Abundant betaines in reef-building corals and ecological indicators of a photoprotective role. *Coral Reefs* 29:869–880.
15. Westmoreland LSH, Niemuth JN, Gracz HS, Stoskopf MK (2017) Altered acrylic acid concentrations in hard and soft corals exposed to deteriorating water conditions. *FACETS* 2:531–544.
16. Blunden G, Guiry MD, Druehl LD, Kogame K, Kawai H (2012) Trigonelline and other betaines in species of Laminariales. *Nat Prod Commun* 7:863–865.
17. Keller MD, Kiene RP, Matrai PA, Bellows WK (1999) Production of glycine betaine and dimethylsulfoniopropionate in marine phytoplankton. I. Batch cultures. *Mar Biol* 135: 237–248.
18. Gebser B, Pohnert G (2013) Synchronized regulation of different zwitterionic metabolites in the osmoadaption of phytoplankton. *Mar Drugs* 11:2168–2182.
19. Goldmann A, et al. (1991) Betaine use by rhizosphere bacteria: Genes essential for trigonelline, stachydrine, and carnitine catabolism in *Rhizobium meliloti* are located on pSym in the symbiotic region. *Mol Plant Microbe Interact* 4:571–578.
20. Boivin C, Camut S, Malpica CA, Truchet G, Rosenberg C (1990) Rhizobium meliloti genes encoding catabolism of trigonelline are induced under symbiotic conditions. *Plant Cell* 2:1157–1170.
21. Boivin C, Barran LR, Malpica CA, Rosenberg C (1991) Genetic analysis of a region of the Rhizobium meliloti pSym plasmid specifying catabolism of trigonelline, a secondary metabolite present in legumes. *J Bacteriol* 173:2809–2817.
22. Young DM, Parke D, Ornston LN (2005) Opportunities for genetic investigation afforded by Acinetobacter baylyi, a nutritionally versatile bacterial species that is highly competent for natural transformation. *Annu Rev Microbiol* 59:519–551.
23. de Berardinis V, Durot M, Weissenbach J, Salanoubat M (2009) Acinetobacter baylyi ADP1 as a model for metabolic system biology. *Curr Opin Microbiol* 12:568–576.
24. Metzgar D, et al. (2004) Acinetobacter sp. ADP1: An ideal model organism for genetic analysis and genome engineering. *Nucleic Acids Res* 32:5780–5790.
25. de Berardinis V, et al. (2008) A complete collection of single-gene deletion mutants of *Acinetobacter* baylyi ADP1. *Mol Syst Biol* 4:174–189.
26. Meade HM, Long SR, Ruvkun GB, Brown SE, Ausubel FM (1982) Physical and genetic characterization of symbiotic and auxotrophic mutants of Rhizobium meliloti induced by transposon Tn5 mutagenesis. *J Bacteriol* 149:114–122.
27. Latypova E, et al. (2010) Genetics of the glutamate-mediated methylamine utilization pathway in the facultative methylotrophic beta-proteobacterium Methyloversatilis universalis FAM5. *Mol Microbiol* 75:426–439.
28. Tautenhahn R, Patti GJ, Rinehart D, Siuzdak G (2012) XCMS online: A web-based platform to process untargeted metabolomic data. *Anal Chem* 84:5035–5039.
29. Loh KD, et al. (2006) A previously undescribed pathway for pyrimidine catabolism. *Proc Natl Acad Sci USA* 103:5114–5119.
30. Ellis HR (2010) The FMN-dependent two-component monooxygenase systems. *Arch Biochem Biophys* 497:1–12.
31. Wright KA, Cain RB (1972) Microbial metabolism of pyridinium compounds. Metabolism of 4-carboxy-1-methylpyridinium chloride, a photolytic product of paraquat. *Biochem J* 128:543–559.
32. Watson GK, Cain RB (1975) Microbial metabolism of the pyridine ring. Metabolic pathways of pyridine biodegradation by soil bacteria. *Biochem J* 146:157–172.
33. Watson GK, Cain RB (1972) Metabolism of pyridine by bacteria. *Biochem J* 127:44P.
34. Faustino H, Alonso I, Mascareñas JL, López F (2013) Gold(I)-catalyzed cascade cycloadditions between allenamides and carbonyl-tethered alkenes: An enantioselective approach to oxa-bridged medium-sized carbocycles. *Angew Chem Int Ed Engl* 52: 6526–6530.
35. Sucharitakul J, et al. (2007) Kinetics of a two-component p-hydroxyphenylacetate hydroxylase explain how reduced flavin is transferred from the reductase to the oxygenase. *Biochemistry* 46:8611–8623.
36. Uetz T, Schneider R, Snozzi M, Egli T (1992) Purification and characterization of a two-component monooxygenase that hydroxylates nitrilotriacetate from "Chelatobacter" strain ATCC 29600. *J Bacteriol* 174:1179–1188.
37. Phongsak T, et al. (2012) The C-terminal domain of 4-hydroxyphenylacetate 3-hydroxylase from Acinetobacter baumannii is an autoinhibitory domain. *J Biol Chem* 287:26213–26222.
38. Tanaka F, Yagi K (1979) Cooperative binding of coenzyme in D-amino acid oxidase. *Biochemistry* 18:1531–1536.
39. Louie TM, Xie XS, Xun L (2003) Coordinated production and utilization of FADH2 by NAD(P)H-flavin oxidoreductase and 4-hydroxyphenylacetate 3-monooxygenase. *Biochemistry* 42:7509–7517.
40. Galán B, Díaz E, Prieto MA, García JL (2000) Functional analysis of the small component of the 4-hydroxyphenylacetate 3-monooxygenase of Escherichia coli W: A prototype of a new flavin:NAD(P)H reductase subfamily. *J Bacteriol* 182:627–636.
41. Jeffers CE, Nichols JC, Tu SC (2003) Complex formation between Vibrio harveyi luciferase and monomeric NADPH:FMN oxidoreductase. *Biochemistry* 42:529–534.
42. Abdurachim K, Ellis HR (2006) Detection of protein-protein interactions in the alkanesulfonate monooxygenase system from Escherichia coli. *J Bacteriol* 188:8153–8159.
43. Valton J, Filisetti L, Fontecave M, Nivière V (2004) A two-component flavin-dependent monooxygenase involved in actinorhodin biosynthesis in Streptomyces coelicolor. *J Biol Chem* 279:44362–44369.
44. Kirchner U, Westphal AH, Müller R, van Berkel WJ (2003) Phenol hydroxylase from Bacillus thermoglucosidasius A7, a two-protein component monooxygenase with a dual role for FAD. *J Biol Chem* 278:47545–47553.
45. Valton J, Fontecave M, Douki T, Kendrew SG, Nivière V (2006) An aromatic hydroxylation reaction catalyzed by a two-component FMN-dependent monooxygenase. The ActVA-ActVB system from Streptomyces coelicolor. *J Biol Chem* 281:27–35.
46. Eichhorn E, van der Ploeg JR, Leisinger T (1999) Characterization of a two-component alkanesulfonate monooxygenase from Escherichia coli. *J Biol Chem* 274:26639–26646.
47. Xun L, Sandvik ER (2000) Characterization of 4-hydroxyphenylacetate 3-hydroxylase (HpaB) of Escherichia coli as a reduced flavin adenine dinucleotide-utilizing monooxygenase. *Appl Environ Microbiol* 66:481–486.
48. Cobessi D, et al. (1999) Apo and holo crystal structures of an NADP-dependent aldehyde dehydrogenase from Streptococcus mutans. *J Mol Biol* 290:161–173.
49. Mukherjee T, Hilmey DG, Begley TP (2008) PLP catabolism: Identification of the 2-(acetamidomethylene)succinate hydrolase gene in Mesorhizobium loti MAFF303099. *Biochemistry* 47:6233–6241.
50. Bakolitsa C, et al. (2010) Structures of the first representatives of Pfam family PF06684 (DUF1185) reveal a novel variant of the Bacillus chorismate mutase fold and suggest a role in amino-acid metabolism. *Acta Crystallogr Sect F Struct Biol Cryst Commun* 66: 1182–1189.

51. Fetzner S (1998) Bacterial degradation of pyridine, indole, quinoline, and their derivatives under different redox conditions. *Appl Microbiol Biotechnol* 49:237–250.
52. Jiménez JI, et al. (2008) Deciphering the genetic determinants for aerobic nicotinic acid degradation: The nic cluster from Pseudomonas putida KT2440. *Proc Natl Acad Sci USA* 105:11329–11334.
53. Bar-Even A, Flamholz A, Noor E, Milo R (2012) Rethinking glycolysis: On the biochemical logic of metabolic pathways. *Nat Chem Biol* 8:509–517.
54. von Stockar U, Maskow T, Liu J, Marison IW, Patiño R (2006) Thermodynamics of microbial growth and metabolism: An analysis of the current situation. *J Biotechnol* 121:517–533.
55. Kaiser JP, Feng Y, Bollag JM (1996) Microbial metabolism of pyridine, quinoline, acridine, and their derivatives under aerobic and anaerobic conditions. *Microbiol Rev* 60:483–498.
56. Jensen RA (1976) Enzyme recruitment in evolution of new function. *Annu Rev Microbiol* 30:409–425.
57. Khersonsky O, Tawfik DS (2010) Enzyme promiscuity: A mechanistic and evolutionary perspective. *Annu Rev Biochem* 79:471–505.
58. Chaiyen P (2010) Flavoenzymes catalyzing oxidative aromatic ring-cleavage reactions. *Arch Biochem Biophys* 493:62–70.
59. Chaiyen P, Brissette P, Ballou DP, Massey V (1997) Reaction of 2-methyl-3-hydroxypyridine-5-carboxylic acid (MHPC) oxygenase with N-methyl-5-hydroxynicotinic acid: Studies on the mode of binding, and protonation status of the substrate. *Biochemistry* 36: 13856–13864.
60. Orpin CG, Knight M, Evans WC (1972) The bacterial oxidation of N-methylisonicotinate, a photolytic product of paraquat. *Biochem J* 127:833–844.
61. Baba T, et al. (2006) Construction of Escherichia coli K-12 in-frame, single-gene knockout mutants: The Keio collection. *Mol Syst Biol* 2:2006.0008.
62. Kobayashi K, et al. (2003) Essential Bacillus subtilis genes. *Proc Natl Acad Sci USA* 100: 4678–4683.
63. Liberati NT, et al. (2006) An ordered, nonredundant library of Pseudomonas aeruginosa strain PA14 transposon insertion mutants. *Proc Natl Acad Sci USA* 103:2833–2838.
64. Denger K, et al. (2014) Sulphoglycolysis in Escherichia coli K-12 closes a gap in the biogeochemical sulphur cycle. *Nature* 507:114–117.
65. Vallenet D, et al. (2017) MicroScope in 2017: An expanding and evolving integrated resource for community expertise of microbial genomes. *Nucleic Acids Res* 45: D517–D528.